



HHS Public Access

Author manuscript

ACS Chem Biol. Author manuscript; available in PMC 2023 August 29.

Published in final edited form as:

ACS Chem Biol. 2022 July 15; 17(7): 1714–1722. doi:10.1021/acscchembio.1c00961.

Discovery of a Redox-Activatable Chemical Probe for Detection of Cyclooxygenase-2 in Cells and Animals

Md. Jashim Uddin^{§,*}, Justin Han-Je Lo^{§,ϕ}, Connor G. Oltman[§], Brenda C. Crews[§], Tamanna Huda[§], Justin Liu^{§,℞}, Philip J. Kingsley[§], Shuyang Lin[§], Mathew Milad[§], Ansari M. Aleem[§], Abu Asaduzzaman[‡], J. Oliver McIntyre^ϙ, Craig L. Duvall^ϙ, Lawrence J. Marnett^{†,*}

[§]Department of Biochemistry, Vanderbilt University, Nashville, Tennessee 37232 USA

^ϕDivision of Hematology and Oncology, Department of Medicine, Vanderbilt University Medical Center, Nashville, TN 37232 USA

[℞]Department of Neuroscience, Columbia University, New York City, New York, 10027 USA

[‡]Department of Electrical Engineering and Computer Science, Wichita State University, Wichita, Kansas 67260 USA

^ϙDepartments of Radiology and Radiological Sciences, and Pharmacology, Vanderbilt Institute of Imaging Science, Vanderbilt University School of Medicine, Nashville, Tennessee 37232 USA

^ϙDepartment of Biomedical Engineering, Vanderbilt University, Nashville, Tennessee 37232 USA

[†]Departments of Biochemistry, Chemistry, and Pharmacology, Vanderbilt Institute of Chemical Biology, Vanderbilt-Ingram Cancer Center, Vanderbilt University School of Medicine, Nashville, Tennessee 37232 USA

Abstract

Cyclooxygenase-2 (COX-2) expression is up-regulated in inflammatory tissues and many premalignant and malignant tumors. Assessment of COX-2 protein in vivo, therefore, promises to be a powerful strategy to distinguish pathologic cells from normal cells in a complex disease setting. Herein, we report the first redox-activatable COX-2 probe, fluorocoxib Q (FQ), for in vivo molecular imaging of pathogenesis. FQ inhibits COX-2 selectively in purified enzyme and cell-based assays. FQ exhibits extremely low fluorescence and displays time- and concentration-dependent fluorescence enhancement upon exposure to a redox environment. FQ enters the cells freely and binds to COX-2 enzyme. FQ exhibits high circulation half-life and metabolic stability sufficient for target site accumulation and demonstrates COX-2-targeted uptake and retention in cancer cells and pathologic tissues. Once taken up, it undergoes redox-mediated transformation

*Corresponding Authors, Md. Jashim Uddin, Ph.D., phone: 615-484-8674, jashim.uddin@vanderbilt.edu, and Lawrence J. Marnett, Ph.D., larry.marnett@vanderbilt.edu.

AUTHOR CONTRIBUTIONS. M.J.U. designed and developed the scale-up procedures for chemical synthesis of fluorocoxib Q (FQ) and fluorocoxib Q-H (FQ-H), designed cell-based assays and performed animal experiments, interpreted the experimental results, and wrote the manuscript. J.H.L., C.G.O., T.H. and J.L. conducted the large-scale synthesis and prep-HPLC purification of FQ and FQ-H. B.C.C. performed cell-based COX-2 inhibition assays, fluorescence microscopy of cancer cells and in vivo pharmacokinetic assay. P.J.K. performed LC-MS analysis of plasma samples. S.L., M.M., and A.M.A. assisted M.J.U. evaluating redox-mediated fluorescence activation of FQ. A.A. performed image analyses and quantified light emission at the regions of interest compared to the control. J.O.M. determined the photophysical properties. C.L.D. provided support for in vivo imaging. L.J.M. conceived of the approach, supervised the overall conduct of the research, edited the manuscript and was responsible for the financial support for the study.

into a fluorescent compound (FQ-H) that results in high signal-to-noise contrast and differentiates pathologic tissues from non-pathologic tissues for real time in vivo imaging.

Keywords

Fluorocoxib Q; COX-2; redox; activatable; inflammation imaging

INTRODUCTION

Cyclooxygenases (COXs) catalyze the *bis*-dioxygenation of arachidonic acid to the hydroperoxy endoperoxide, prostaglandin G₂ (PGG₂) and the subsequent reduction of the hydroperoxy group of PGG₂ to an alcohol, yielding prostaglandin H₂ (PGH₂).^{1, 2} PGH₂ represents a branch point in the biosynthetic pathway that leads to the formation of prostaglandins, thromboxane, or prostacyclin. These compounds function in a wide range of physiological and pathophysiological responses including platelet aggregation, gastric cytoprotection, inflammation, and hyperalgesia.^{3, 4} Thus, COXs play a key role in the generation of a broad array of bioactive lipids.

There are two COX genes that code for structurally related proteins that are approximately 60% identical in amino acid sequence.⁵⁻⁷ In general, the COX-1 gene is constitutively expressed in multiple tissues, although there are a few examples where its expression is inducible (e.g., during differentiation of cultured cells in vitro).⁸ The COX-2 gene is highly regulated, and its expression is triggered by a broad array of cytokines, growth factors, and tumor promoters, leading to a strong association between this isoform and preneoplastic, neoplastic, and/or inflammatory tissues.⁹⁻¹¹ For example, studies have demonstrated that COX-2 mRNA and protein are expressed in a wide range of cancerous and precancerous lesions, including those of the esophagus, breast, bladder, lung, and skin.¹²⁻¹⁷ In the colon, COX-2 is detectable in tumor material from cancer patients but not in surrounding normal tissue.^{18, 19} COX-2 expression appears to be an early event in colon tumorigenesis because it is detectable in colon polyps.^{20, 21} Due to its overexpression in inflamed and neoplastic tissues and relative scarcity in normal tissues, COX-2 is an attractive molecular target for diagnostic imaging in a variety of clinical settings. For example, detecting molecular biomarkers associated with the initiation and progression of neoplastic diseases facilitates early detection followed by timely surgical/therapeutic intervention.²²⁻²⁴ Similarly, the use of imaging for the intraoperative analysis of margins during surgical procedures can assist the detection of cancer at those margins, thereby reducing the incidence of inadequate surgical removal of some malignant lesions.²⁵⁻²⁷

We have previously described the synthesis and in vivo validation of COX-2-targeted radiologic imaging agents for both single photon emission tomography and positron emission tomography imaging.²⁸⁻³⁰ We have also reported the development of fluorocoxibs, a series of COX-2-targeted fluorescent imaging agents based on the conjugation of the COX inhibitor indomethacin with rhodamine dyes. Fluorocoxibs enable in vivo imaging of COX-2 in multiple animal models of premalignant and malignant tumors and inflammation.³¹⁻³⁶ Of these agents, fluorocoxib A (FA) is the most thoroughly investigated imaging agent

by us,^{31, 34, 37-39} and others.⁴⁰⁻⁴⁴ It has been shown to have adequate in vivo stability and pharmacokinetic properties to remain intact in the circulation and to accumulate in inflammatory tissues or tumors. Additionally, its fluorescence properties are suitable for detection with minimal autofluorescence interference.⁴⁵

An alternative approach to COX-2-targeted imaging is the use of activatable agents, which would only be detectable upon sensing certain condition, such as the redox environment of the target site. Such agents would theoretically increase target site accumulation by COX-2 binding and improve the signal-to-noise due to a substantial reduction in background. A number of such agents have been reported in the literature for COX-2-targeted fluorescence imaging, including ANQ-IMC-6 and CoxFlour.^{46, 47} Although selective uptake of these agents into intact cells expressing COX-2 has been demonstrated in vitro, in vivo tumor imaging has not been reported. Herein, we report the discovery of fluorocoxib Q, the first redox-activatable COX-2 probe, which overcomes the limitations of previously reported activatable COX-2 probes allowing in vitro and in vivo detection of COX-2 in intact cells and live animals.

RESULTS AND DISCUSSION

Design of Redox-Activatable COX-2 Probes.

COX-2 has both an oxygenase activity that makes the PGG₂ hydroperoxide product and a peroxidase activity that reduces the hydroperoxide while concomitantly generating an oxidant. Consequently, studies have shown that COX-2 activity is associated with the production of reactive oxygen species (ROS) leading to oxidative stress, as indicated by the generation of DNA damage.⁴⁸ Furthermore, oxidative stress enhances the expression of nuclear factor kappa-B (NF- κ B), which, in turn induces increased COX-2 expression in pathological tissues.^{49, 50} We hypothesize that COX-2 and ROS co-localize in inflammatory and tumor cells. Thus, redox-activatable COX-2 probes can enhance the detection and contrast of the margins of pathologic lesions from the surrounding non-pathologic normal tissues.

Development of the Redox-Activatable Chemical Probe.

Studies have shown that nitroxide radicals are capable of spin trapping and spin labeling in electron paramagnetic resonance spectroscopy.⁵¹⁻⁵³ These antioxidant species enable the monitoring of cellular redox processes.⁵⁴⁻⁵⁹ Due to our high level of success with fluorocoxib A (FA), we chose it as the scaffold for our redox-activatable probe. The fluorescence of FA's rhodamine moiety can be quenched by conjugating a nitroxide radical to it.⁶⁰ Conjugation of an amino-TEMPO molecule to the carboxylic acid of FA via an amide linkage resulted in a molecule we call fluorocoxib Q (FQ). We synthesized the starting FA using our published procedure.³¹ Then, for conjugation of the nitroxide functional group, we created a mixed-anhydride at the carboxyl substituent of the rhodamine moiety that successfully reacted with the amino group of 4-amino-TEMPO to afford FQ (Fig. 1). The FQ and its reduced hydroxylamine analog fluorocoxib Q-H (FQ-H) were purified by HPLC (Fig. S1,S2) and characterized by spectroscopic analyses (Fig. S3-S6).

Redox-Mediated Fluorescence Activation of FQ.

Treatment of FQ with sodium ascorbate (1:1) resulted in a time- and concentration-dependent increase in the intensity of fluorescence emission ($\lambda_{em} = 607$ nm) (Fig. 2a,b). Iron is closely associated with Fenton's or Haber-Weiss's chemistry, which catalyzes the production of hydroxyl radicals.^{61, 62} Studies have shown that in place of Fe^{2+} , Cu^{2+} can also be used to produce hydroxyl radicals that can induce the transformation of pro-fluorescent nitroxides into fluorescent hydroxylamines.⁶⁰ We treated FQ with Fenton's reagent (10-fold excess of $FeSO_4$ and 100-fold excess of H_2O_2 relative to FQ) that produced a much stronger fluorescence emission than that of untreated FQ (Fig. 2c). We evaluated the photophysical properties of FQ and observed a reduced quantum yield ($\Phi_{fl} < 0.19$ at 607 nm) and extinction coefficient ($\epsilon < 0.4$ $mM^{-1}cm^{-1}$ at 586 nm) compared to that of the parent FA ($\Phi_{fl} = 0.93$ at 602 nm, $\epsilon = 45$ $mM^{-1}cm^{-1}$ at 579 nm) or FQ-H ($\Phi_{fl} = 0.90$ at 607 nm, $\epsilon = 44$ $mM^{-1}cm^{-1}$ at 586 nm) (Fig. 2d). FQ's low fluorescence is accounted for by quenching of the excited electronic state of its fluorophore, carboxy-X-rhodamine, by the nitroxide radical within the molecule, and it is likely that the quenching is attributable to a photoinduced electron transfer from nitroxide radical to the carboxy-X-rhodamine fluorophore in the excited state.⁶⁰

In Vitro Purified COX Isozyme Inhibition Assays.

We evaluated the ability of FQ and FQ-H to selectively inhibit COX-2, as opposed to COX-1, using purified isozymes with ^{14}C -arachidonic acid as a substrate.³¹ Both compounds showed selective and potent inhibition of COX-2 (IC_{50} values of 0.33 μM and 0.24 μM for FQ and FQ-H, respectively, as compared to >4 μM for COX-1) (Fig. 3a,b). Note that the failure of FQ and FQ-H to completely inhibit COX-2 at high concentrations is an indication that the compounds most likely act by binding in the allosteric subunit rather than the catalytic subunit of the dimeric enzyme.⁶³

Cell-based COX-2 Inhibition Assay.

We evaluated the COX-2 inhibitory activity of both FQ and FQ-H in intact cells using the 1483 head and neck squamous cell carcinoma (HNSCC) cell line. This cell line expresses elevated levels of COX-2 (Fig. 3c,d).³¹ Both FQ and FQ-H showed potent cellular COX-2 inhibition with IC_{50} values of 0.28 μM and 0.26 μM , respectively.

Cell Imaging Assay.

We evaluated FQ's ability to image 1483 HNSCC cells containing high COX-2 expression. After treating cells with FQ followed by washout, we performed fluorescence microscopy of the treated cells at 0.5 and 3 h post-addition of compound. The optical imaging showed low fluorescence intensity at the earlier (0.5 h) time point, however strong fluorescence was detected at the later (3 h) time point due to the accumulation and fluorescence activation of FQ in 1483 HNSCC cells (Fig. 3e-g). In addition, we performed an experiment to test whether fluorocoxib Q-H's fluorescence labeling of 1483 HNSCC cells is COX-2 dependent. Cells were pretreated with vehicle or celecoxib to block the COX-2 active site prior to the treatment with fluorocoxib Q-H. After repetitive washing, cells were imaged. The 1483 HNSCC cells treated with fluorocoxib Q-H alone exhibited strong perinuclear

fluorescence (Fig. S7a) that was blocked by preincubation with the COX-2 inhibitor celecoxib (Fig. S7b), suggesting that the fluorescence labeling is COX-2 dependent.

In Vivo Pharmacokinetic Assay.

We evaluated the pharmacokinetic properties of FQ in CD-1 mice. Mice were dosed and plasma collected and processed as described in the Materials and Methods section (Fig. 4a, b). The results indicated that the FQ molecule can remain in the circulation for adequate periods of time to enable it to reach the target site in vivo.

Redox-Mediated Detection of COX-2 in Inflammation.

We evaluated the ability of FQ for the detection of COX-2 in the presence of endogenously generated ROS using a murine model of carrageenan-induced acute inflammation. Acute inflammation in the right hind footpad of C57BL/6 mice was induced by a single subcutaneous injection of 1% λ -carrageenan dissolved in sterile saline.³⁴ First, we used luminol for chemiluminescence imaging of ROS in this model. Studies have shown that luminol reacts with ROS within biological systems to produce an excited state of 3-aminophthalate, which then releases a photon as it returns to the ground state.^{64, 65} We dosed mice with luminol 6 h following carrageenan injection. Chemiluminescence imaging was performed for data acquisition periods of 1 min beginning at 5 min post-luminol injection. A focal and significantly distinct chemiluminescence emission was detected in the inflamed footpads (mean \pm sd = 1251.5 \pm 94.9, $p < 0.0004$, $n = 8$). This luminescence was 12-fold higher than that from control footpads, confirming high endogenous ROS production in carrageenan-induced inflammation. To further confirm the specificity of luminol, the ROS scavenging agent TEMPOL was injected prior to the administration of luminol. The pre-administration of TEMPOL resulted in a significant reduction of the chemiluminescence signal from the carrageenan-treated footpads, suggesting that the signal was indeed generated by endogenous ROS (Fig. 4c). Elevated COX-2 expression is a hallmark of carrageenan-induced inflammation in the footpad model, and COX-2-derived prostaglandins play a major role in inducing the footpad edema.^{29, 30, 66} We evaluated the utility of FQ in the visualization of ROS and COX-2 co-localization in this acute paw inflammation model. After dosing by intraperitoneal injection, FQ appeared to be taken up, converted into fluorescent FQ-H by ROS, and retained at the site of inflammation by binding to COX-2, thereby enabling visualization of inflamed lesions. The optical imaging afforded an average 9-fold increase in fluorescence in the inflamed (mean \pm sd = 7.84 $\times 10^8 \pm 1.25 \times 10^8$, $p < 0.001$, $n = 8$) over the non-inflamed footpads (Fig. 4d). The targeting was significantly blocked by pre-injection of either the ROS scavenger TEMPOL or the COX-2-selective inhibitor celecoxib, supporting our proposed mode of action.

These studies suggest that FQ targets both COX-2 and ROS in pathologic tissues. To evaluate whether FQ possesses any advantage over our previous compounds, those that target COX-2 alone, we compared the ability of FQ versus CF₃-FA³³ in molecular imaging of carrageenan-induced footpad inflammation of wild-type C57BL/6 mice. After imaging, mice injected with CF₃-FA showed a fluorescence signal in their inflamed footpad with some unavoidable background signals in the non-inflamed footpad as well. In contrast, mice injected with FQ showed fluorescence signal only at their inflamed footpad with an

extremely low background signal in the non-inflamed footpad. The negligible background signal of FQ in non-inflamed footpad is attributable to the lack of ROS/COX-2 in non-inflamed normal footpad tissues. As a result, FQ enables *in vivo* molecular imaging with reduced background noise (Fig. S8a-c). It is possible that in the inflammatory lesions, the nitroxide radical of FQ is converted into a transient nitrosonium ion intermediate by an electron transfer to ROS, such as a peroxy radical.⁶⁷ Then in presence of a hydride donor, such as NADPH, the nitrosonium ion intermediate is converted into the stable hydroxyamine product FQ-H.⁶⁸

In conclusion, we report the discovery of FQ, the first redox-activatable COX-2 probe for *in vivo* imaging of pathogenesis. FQ is a conjugate of the nonsteroidal anti-inflammatory drug indomethacin and a carboxy-X-rhodamine fluorophore bearing the quenching nitroxide, 4-amino-TEMPO. In its inactivated state, FQ exhibits extremely low fluorescence. FQ becomes fluorescent upon exposure to reactive oxygen species in a redox environment, then binds in the COX-2 active site. FQ detects the presence of COX-2 in cultured cancer cells and in a mouse model of carrageenan-induced inflammation *in vivo*. The combination of molecular targeting with intracellular activation circumvents the presence of extracellular, nonspecific signals of targeted probe accumulation. This strategy will greatly improve sensitivity and specificity of detection and potentially provides enhanced and high contrast delineation of pathological versus normal tissues for the visualization of a broad range of neoplastic and inflammatory conditions in the clinical setting.

METHODS

Chemistry.

We utilized standard methods for chemical synthesis of fluorocoxib A.³¹ The carboxylic acid located on the backbone of the carboxy-x-rhodamine group of fluorocoxib A was tethered to a nitroxide radical through an amide bond to give fluorocoxib Q, which was treated with ascorbic acid or Fenton's reagent to produce fluorocoxib Q-H.

Synthesis of Fluorocoxib Q:

To a stirred solution of fluorocoxib A (20 mg, 0.02 mmol) in tetrahydrofuran (2.5 mL) was added triethylamine (3 mg, 0.03 mmol) and ethylchloroformate (10 mg, 0.1 mmol). Following stirring for 1h at -15°C , 4-amino-TEMPO (20 mg, 0.12 mmol) was added at -15°C , and the resulting solution was stirred for 16 h at -15°C to room temperature. The solvent was evaporated *in vacuo* to dryness, and the crude product was purified by silica gel column chromatography (chloroform/methanol/ammonium hydroxide, 35:7:1, v/v/v) to give the pure fluorocoxib Q as a brown solid (14 mg, 62% yield, purity 99% on HPLC). ^1H NMR (600 MHz, dimethyl sulfoxide- d_6) δ 0.93-0.97 (m, 4H), 1.32-1.37 (m, 16H), 1.59-1.65 (m, 4H), 1.85-1.90 (m, 4H), 2.14-2.20 (m, 2H), 2.32 (s, 3H), 2.59-2.60 (m, 3H), 2.90-2.95 (m, 2H), 3.12-3.21 (m, 8H), 3.22-3.28 (m, 6H), 3.59 (s, 2H), 3.83 (s, 3H), 5.77 (s, 2H), 6.77-6.78 (m, 1H), 7.02-7.03 (m, 1H), 7.21 (s, 1H), 7.30-7.35 (m, 1H), 7.73-7.78 (m, 4H), 7.79-7.80 (m, 1H), 8.14-8.18 (m, 2H), 8.25-8.26 (m, 1H), 8.82-8.83 (br s, 1H). ^{13}C NMR (150 MHz, dimethyl sulfoxide- d_6) 0.92(2C), 13.37(2C), 13.95(3C), 16.80(3C), 22.81(4C), 26.53(2C), 26.70(2C), 28.83(4C), 29.06(5C), 31.20(3C), 32.79(3C), 38.49

(3C), 48.59(3C), 49.19(3C), 55.41(2C), 101.80(2C), 114.43(2C), 129.03(4C), 130.26(4C), 131.14(4C), 137.54(2C), 155.52(2C), 167.84. HRMS calcd for $C_{65}H_{72}ClN_7O_7^{*+}$ (M^{*+}) 1097.5176; found 1097.5169.

Synthesis of Fluorocoxib Q-H:

To a stirred solution of sodium L-ascorbate (1.98 mg, 0.01 mmol) in 1 mL methanol: water (1:1) was added fluorocoxib Q (6.58 mg, 0.006 mmol), and the resulting solution was stirred 48 h at 25 °C. Dichloromethane (1 mL) was added to the reaction mixture and the product was extracted three times. The combined organic layer was washed with water and brine, then the solvent was evaporated *in vacuo* after treatment with anhydrous sodium sulfate. The crude product was purified by silica gel column chromatography (chloroform/methanol/ ammonium hydroxide, 35:7:1, v/v/v) to afford pure fluorocoxib Q-H as a dark violet solid (3.6 mg, 50% yield, purity 99% on HPLC). 1H NMR (600 MHz, dimethyl sulfoxide- d_6) δ 0.84-0.89 (m, 4H), 1.16 (s, 12H), 1.42-1.44 (m, 4H), 1.65-1.70 (m, 4H), 1.82 (s, 2H), 1.85-1.87 (m, 2H), 2.15-2.17 (m, 2H), 2.20 (s, 3H), 2.30-2.37 (m, 4H), 2.72-2.77 (m, 4H), 3.03-3.08 (m, 4H), 3.40 (s, 2H), 2.55-2.60 (m, 4H), 3.65 (s, 3H), 3.82-3.83 (m, 2H), 3.94-3.95 (m, 2H), 5.75 (s, 2H), 6.61 (dd, $J=9.3, 2.4$ Hz, 1H), 6.85 (d, $J=9.4$ Hz, 1H), 6.96 (br s, 1H), 7.04 (d, $J=2.4$ Hz, 1H), 7.15 (d, $J=9.2$ Hz, 1H), 7.55 (d, $J=8.6$ Hz, 2H), 7.60 (d, $J=8.6$ Hz, 2H), 7.95-7.98 (m, 2H), 8.12 (s, 1H), 8.62-8.64 (m, 1H). ^{13}C NMR (150 MHz, dimethyl sulfoxide- d_6). 11.95(2C), 13.86, 14.43, 18.94, 21.23(2C), 21.39(2C), 21.66, 22.04, 22.56(2C), 24.91(2C), 27.17, 29.17(2C), 29.49(3C), 31.68, 31.76, 32.89, 33.95(2C), 46.12, 49.23, 49.66(2C), 55.87, 58.39, 63.09(2C), 65.95(2C), 69.75(2C), 102.28(2C), 105.59, 107.39, 111.75(2C), 114.91, 115.01(2C), 117.50, 124.39, 129.49, 130.73, 131.37, 131.61, 134.74, 135.56, 138.00, 143.87, 148.49, 156.00, 168.32, 169.74, 172.57(2C), 173.45(2C). HRMS calcd for $C_{65}H_{73}ClN_7O_7$ (M^+) 1098.5255; found 1098.5262.

Redox-Mediated Fluorescence Activation Assays.

We treated pro-fluorescent fluorocoxib Q with sodium L-ascorbate or Fenton's reagent for fluorescence activation. The activated fluorescence was measured fluorometrically. (a) Treatment with Sodium L-Ascorbate: To a stirred solution of sodium L-ascorbate (0.0198 mg, 0.0001 mmol) in methanol:water (v/v 1:1, 2.5 mL) was added fluorocoxib Q (0.1097 mg, 0.0001 mmol) at 25 °C. The fluorescence emission of the solution was measured on a Spex 1681 Fluorolog fluorescence spectrophotometer starting at 6 min post-fluorocoxib Q addition, followed by measuring every 6 min up to 72 min. (b) Sodium L-Ascorbate Concentration Dependence: Using the procedure described above, fluorocoxib Q was treated with a 10-fold, 100-fold, or 1000-fold excess of sodium L-ascorbate at 25 °C. The fluorescence emission of the reaction mixtures was measured fluorometrically at 1 h post-treatment. (c) Treatment with Fenton Reagent: To a stirred solution of fluorocoxib Q (1.1 mg, 0.001 mmol) in Dulbecco's phosphate buffered saline pH 4 (0.5 mL) was added a solution of ferrous sulfate heptahydrate (2.78 mg, 0.01 mmol) in water (0.5 mL) followed by hydrogen peroxide (30% w/w, 1.2 mL ($H_2O_2 = 0.36$ mg, 0.01 mmol)). After 30 min of gentle stirring at 25°C, the fluorescence emission of the reaction was measured using a Spex 1681 Fluorolog fluorescence spectrophotometer. Using identical conditions, the emission intensity of a control solution was measured in which fluorocoxib Q was kept untreated.

Photophysical Properties.

The photophysical properties of fluorocoxib Q and fluorocoxib Q-H were measured fluorometrically on a photon counting Fluorometer using Felix software. Fluorocoxib A was used as a standard for comparison to calculate optical properties of each sample. All measurements were performed in a 10 x 4 mm cuvette at 25 °C. Samples were diluted to 1 μ M before each measurement. Fluorescence excitation and emission spectra of fluorocoxib Q, fluorocoxib Q-H and fluorocoxib A were recorded in triplicates. The quantum yield (ϕ) of each sample was calculated by comparing one's fluorescence with the fluorescence of properties fluorocoxib A. The extinction coefficient (ϵ) of each sample was calculated from one's absorbance spectra taken in a 10 mm pathlength cuvette at a series of 10, 8, 6, 4, and 2 μ M dilutions on a UV-VIS spectrophotometer.

Purified Isozyme Inhibition Assay.

Purified COX-1 and COX-2 inhibitory activities of fluorocoxib Q and fluorocoxib Q-H were determined using a thin-layer chromatography (TLC) assay, in which hematin-reconstituted purified COX-1 (44 nmol/L) or COX-2 (66 nmol/L) in 100 mM Tris-HCl containing 500 μ M phenol at pH 8.0 were preincubated with varying concentrations of fluorocoxib Q or fluorocoxib Q-H dissolved in dimethylsulfoxide at 25 °C for 17 min and 37 °C for 3 min followed by the addition of the radio-labeled substrate [14 C]arachidonic acid (50 μ mol/L). Then the reaction mixtures were vortexed for 30 seconds at 37 °C. The reactions were terminated by the addition of ether:methanol:citric acid (30:4:1, pH 4). The aqueous and organic phases were separated by centrifugation. The organic phase was spotted on a TLC plate and developed using a mixed solvent system composed of ethyl acetate:dichloromethane:glacial acetic acid (75:25:1) at 4 °C to separate the radiolabeled prostaglandin products. The radiolabeled products were quantified on a Bioscan Radioactivity Scanner.

Cell Imaging Assay.

1483 HNSCC cells in Hank's balanced salt solution (HBSS)/Tyrode's were grown to a confluency of 50% and incubated with 200 nM of FQ. Following incubation for 0.25 h at 37 °C, cells were washed three times with HBSS/Tyrode's and imaged on a Zeiss Axiovert 25 Fluorescence Microscope with a propidium iodide filter at 0.5 h and 3 h post-addition of FQ. The experiment was performed in triplicates. At each of these time points, FQ-treated 1483 HNSCC cells were imaged on an exposure of 0.5 sec with a gain of 2 and fluorescence intensities were quantified on a BioTek Synergy Mx Plate Reader at an absorbance of 586 nm and emission of 607 nm.

In vivo Pharmacokinetic Assay.

We performed animal experiments using protocols that are approved by the Vanderbilt Institutional Animal Care and Use Committee (IACUC). In an animal experiment, CD-1 mice were dosed with FQ (10 mg/kg, i.p.) and blood samples were collected via cardiac puncture at 0, 0.5, 1, 3, 6 and 24 post-injection (n=3 for each timepoint). The collected blood was centrifuged to obtain plasma and the plasma was stored at -80C until further processing. FQ was purified from the plasma by the acetonitrile-freeze method. Briefly, the

plasma was diluted with Tris (pH 7.0) buffer and an excess of acetonitrile was added. This was mixed well, centrifuged and stored at $-20\text{ }^{\circ}\text{C}$ overnight to promote a phase separation. The following day, separate phases were observed and the upper, organic layer contained which contained FQ was removed to a clean vessel. This was then dried under nitrogen gas, reconstituted and analyzed by LC-MS to determine the FQ levels.

Animal Model for Evaluation of FQ.

The carrageenan-induced mouse footpad inflammation model was employed to evaluate the potential of fluorocoxib Q in imaging inflammatory conditions. The 1% λ -carrageenan solution was prepared by mixing 10 mg λ -carrageenan with 1 mL of a 0.9% injectable solution sodium chloride in a sterile plastic vial. After gentle swirling (5-6 times) the vial was left undisturbed for 16 h at room temperature. The resultant carrageenan solution (50 μL) was injected in the rear right footpad of male and female C57BL/6 mice. Control mice were not injected with carrageenan.

Imaging Reactive Oxygen Species (ROS).

At 6 hours post-carrageenan injection, the first test group (8 animals/group) of animals was dosed with saline, and the 2nd test group (8 animals/group) of animals was dosed with an aqueous saline solution of tempol (5 mg/kg, i.v.). Luminol sodium (5 mg/kg, i.v.) was injected 15 min after dosing of saline or tempol. In addition, the control group (8 animals/group) of animals was dosed with luminol sodium (5 mg/kg, i.v.). At 15 min of post-luminol injection, all animals (carrageenan or no carrageenan) were imaged by whole body chemiluminescence imaging using a Xenogen IVIS 200 instrument. The luminol signals were quantified by ImageJ software via regions of interest (ROIs) measurements.

Redox-Mediated Detection of COX-2 in Inflammation.

For *in vivo* imaging and validation of ROS and COX-2 co-localization, we used three test groups of animals (8 animals/group) with carrageenan-induced footpad inflammation. After 6 h of carrageenan injection, the 1st, 2nd, and 3rd test group of animals were injected with saline, tempol (5 mg/kg, i.p.), or celecoxib (10 mg/kg, i.p.), respectively. Fluorocoxib Q (5 mg/kg, i.p.) was injected 1 h post-dosing of saline, tempol or celecoxib. The control group of animals (8 animals) was dosed with fluorocoxib Q (5 mg/kg, i.p.). Fluorescence imaging was performed on all animals (no carrageenan or carrageenan) at 24 h of post-fluorocoxib Q injection using a Xenogen IVIS 200 instrument. The images were analyzed for the measurement of fluorescence signals at the regions of interest using ImageJ software.

Supplementary Material

Refer to Web version on PubMed Central for supplementary material.

ACKNOWLEDGMENTS.

We thank the Vanderbilt University Institute of Imaging Science for *in vivo* molecular imaging, the Small Molecule NMR facilities and the Mass Spectroscopy Research Center for compound characterization, Dr. Carol A. Rouzer of the Vanderbilt Basic Sciences for critical reading and editing of the manuscript.

FUNDING.

We are thankful to the Vanderbilt Institute for Clinical and Translational Research (VICTR) fund VR52653 (M.J.U.) and the National Institutes of Health (NIH) research grants CA128323-4, -5 (M.J.U.), CA260958-01A1 (M.J.U. and C.L.D.), CA217834 (J.H.L.), and CA89450 (L.J.M.) for financially supporting the study.

ABBREVIATIONS.

COX-2	Cyclooxygenase-2
FA	fluorocoxib A
FQ	fluorocoxib Q
FQ-H	fluorocoxib Q-H
5-ROX	5-carboxy-X-rhodamine
ROS	reactive oxygen species
LC	liquid chromatography
MS	mass spectrometry
NF-κB	nuclear factor kappa-B
PG-G₂	prostaglandin G ₂
PG-H₂	prostaglandin H ₂
mRNA	messenger RNA

REFERENCES

1. Rouzer CA, and Marnett LJ (2003) Mechanism of free radical oxygenation of polyunsaturated fatty acids by cyclooxygenases, *Chem. Rev* 103, 2239–2304. [PubMed: 12797830]
2. Smith WL, Garavito RM, and DeWitt DL (1996) Prostaglandin endoperoxide H synthases (cyclooxygenases)-1 and -2, *J. Biol. Chem* 271, 33157–33160. [PubMed: 8969167]
3. Dubois RN, Abramson SB, Crofford L, Gupta RA, Simon LS, Van De Putte LB, and Lipsky PE (1998) Cyclooxygenase in biology and disease, *FASEB J.* 12, 1063–1073. [PubMed: 9737710]
4. Vane JR, Bakhle YS, and Botting RM (1998) Cyclooxygenases 1 and 2, *Annu. Rev. Pharmacol. Toxicol* 38, 97–120. [PubMed: 9597150]
5. Xie WL, Chipman JG, Robertson DL, Erikson RL, and Simmons DL (1991) Expression of a mitogen-responsive gene encoding prostaglandin synthase is regulated by mRNA splicing, *Proc. Natl. Acad. Sci. USA* 88, 2692–2696. [PubMed: 1849272]
6. Fletcher BS, Kujubu DA, Perrin DM, and Herschman HR (1992) Structure of the mitogen-inducible TIS10 gene and demonstration that the TIS10-encoded protein is a functional prostaglandin G/H synthase, *J. Biol. Chem* 267, 4338–4344. [PubMed: 1339449]
7. Hla T, and Neilson K (1992) Human cyclooxygenase-2 cDNA, *Proc. Natl. Acad. Sci. USA* 89, 7384–7388. [PubMed: 1380156]
8. Smith CJ, Morrow JD, Roberts LJ 2nd, and Marnett LJ (1993) Differentiation of monocytoid THP-1 cells with phorbol ester induces expression of prostaglandin endoperoxide synthase-1 (COX-1), *Biochem. Biophys. Res. Commun* 192, 787–793. [PubMed: 8484784]
9. Herschman HR (1996) Prostaglandin synthase 2, *Biochim. Biophys. Acta* 1299, 125–140. [PubMed: 8555245]

10. Crofford LJ (1997) COX-1 and COX-2 tissue expression: implications and predictions, *J. Rheumatol. Suppl* 49, 15–19. [PubMed: 9249646]
11. Dannenberg AJ, Lippman SM, Mann JR, Subbaramaiah K, and DuBois RN (2005) Cyclooxygenase-2 and epidermal growth factor receptor: pharmacologic targets for chemoprevention, *J. Clin. Oncol* 23, 254–266. [PubMed: 15637389]
12. Kandil HM, Tanner G, Smalley W, Halter S, Radhika A, and Dubois RN (2001) Cyclooxygenase-2 expression in Barrett's esophagus, *Dig. Dis. Sci* 46, 785–789. [PubMed: 11330414]
13. Ristimaki A, Nieminen O, Saukkonen K, Hotakainen K, Nordling S, and Haglund C (2001) Expression of cyclooxygenase-2 in human transitional cell carcinoma of the urinary bladder, *Am. J. Pathol* 158, 849–853. [PubMed: 11238034]
14. Ristimaki A, Sivula A, Lundin J, Lundin M, Salminen T, Haglund C, Joensuu H, and Isola J (2002) Prognostic significance of elevated cyclooxygenase-2 expression in breast cancer, *Cancer Res.* 62, 632–635. [PubMed: 11830510]
15. Tucker ON, Dannenberg AJ, Yang EK, Zhang F, Teng L, Daly JM, Soslow RA, Masferrer JL, Woerner BM, Koki AT, and Fahey TJ 3rd. (1999) Cyclooxygenase-2 expression is up-regulated in human pancreatic cancer, *Cancer Res.* 59, 987–990. [PubMed: 10070951]
16. Soslow RA, Dannenberg AJ, Rush D, Woerner BM, Khan KN, Masferrer J, and Koki AT (2000) COX-2 is expressed in human pulmonary, colonic, and mammary tumors, *Cancer* 89, 2637–2645. [PubMed: 11135226]
17. Denkert C, Kobel M, Berger S, Siegert A, Leclere A, Trefzer U, and Hauptmann S (2001) Expression of cyclooxygenase 2 in human malignant melanoma, *Cancer Res.* 61, 303–308. [PubMed: 11196178]
18. Kargman SL, O'Neill GP, Vickers PJ, Evans JF, Mancini JA, and Jothy S (1995) Expression of prostaglandin G/H synthase-1 and -2 protein in human colon cancer, *Cancer Res.* 55, 2556–2559. [PubMed: 7780968]
19. Eberhart CE, Coffey RJ, Radhika A, Giardiello FM, Ferrenbach S, and DuBois RN (1994) Up-regulation of cyclooxygenase 2 gene expression in human colorectal adenomas and adenocarcinomas, *Gastroenterology* 107, 1183–1188. [PubMed: 7926468]
20. Sheehan KM, Sheahan K, O'Donoghue DP, MacSweeney F, Conroy RM, Fitzgerald DJ, and Murray FE (1999) The relationship between cyclooxygenase-2 expression and colorectal cancer, *JAMA* 282, 1254–1257. [PubMed: 10517428]
21. Peek RM Jr. (2004) Prevention of colorectal cancer through the use of COX-2 selective inhibitors, *Cancer Chemother Pharmacol* 54 Suppl 1, S50–56. [PubMed: 15309515]
22. Raut CP, Tseng JF, Sun CC, Wang H, Wolff RA, Crane CH, Hwang R, Vauthey JN, Abdalla EK, Lee JE, Pisters PW, and Evans DB (2007) Impact of resection status on pattern of failure and survival after pancreaticoduodenectomy for pancreatic adenocarcinoma, *Ann. Surg* 246, 52–60. [PubMed: 17592291]
23. Gao RW, Teraphongphom NT, van den Berg NS, Martin BA, Oberhelman NJ, Divi V, Kaplan MJ, Hong SS, Lu G, Ertsey R, Tummers W, Gomez AJ, Holsinger FC, Kong CS, Colevas AD, Warram JM, and Rosenthal EL (2018) Determination of tumor margins with surgical specimen mapping using near-infrared fluorescence, *Cancer Res.* 78, 5144–5154. [PubMed: 29967260]
24. Nakanishi K, Morita S, Taniguchi H, Otsuki S, Fukagawa T, and Katai H (2019) Diagnostic accuracy and usefulness of intraoperative margin assessment by frozen section in gastric cancer, *Ann. Surg. Oncol* 26, 1787–1794. [PubMed: 30877498]
25. McAuliffe JC, Tang LH, Kamrani K, Olin K, Klimstra DS, Brennan MF, and Coit DG (2019) Prevalence of false-negative results of intraoperative consultation on surgical margins during resection of gastric and gastroesophageal adenocarcinoma, *JAMA Surg.* 154, 126–132. [PubMed: 30422226]
26. Nelson DW, Blanchard TH, Causey MW, Homann JF, and Brown TA (2013) Examining the accuracy and clinical usefulness of intraoperative frozen section analysis in the management of pancreatic lesions, *Am. J. Surg* 205, 613–617; discussion 617. [PubMed: 23592172]
27. Shyn PB, Casadaban LC, Sainani NI, Sadow CA, Bunch PM, Levesque VM, Kim CK, Gerbaudo VH, and Silverman SG (2018) Intraprocedural ablation margin assessment by using ammonia

- perfusion PET during FDG PET/CT-guided liver tumor ablation: a pilot study, *Radiology* 288, 138–145. [PubMed: 29613843]
28. Uddin MJ, Crews BC, Blobaum AL, Kingsley PJ, Ghebreselasie K, Saleh SS, Clanton JA, Baldwin RM, and Marnett LJ (2009) Synthesis and evaluation of [¹²³I]-indomethacin derivatives as COX-2 targeted imaging agents, *Journal of Labelled Compounds and Radiopharmaceuticals* 52, 387–393.
 29. Uddin MJ, Crews BC, Ghebreselasie K, Huda I, Kingsley PJ, Ansari MS, Tantawy MN, Reese J, and Marnett LJ (2011) Fluorinated COX-2 inhibitors as agents in PET imaging of inflammation and cancer, *Cancer Prev. Res* 4, 1536–1545.
 30. Uddin MJ, Crews BC, Ghebreselasie K, Tantawy MN, and Marnett LJ (2011) [I]-Celecoxib analogues as SPECT tracers of cyclooxygenase-2 in inflammation, *ACS Med. Chem. Lett* 2, 160–164. [PubMed: 21318094]
 31. Uddin MJ, Crews BC, Blobaum AL, Kingsley PJ, Gorden DL, McIntyre JO, Matrisian LM, Subbaramaiah K, Dannenberg AJ, Piston DW, and Marnett LJ (2010) Selective visualization of cyclooxygenase-2 in inflammation and cancer by targeted fluorescent imaging agents, *Cancer Res.* 70, 3618–3627. [PubMed: 20430759]
 32. Uddin MJ, Crews BC, Ghebreselasie K, and Marnett LJ (2013) Design, synthesis, and structure-activity relationship studies of fluorescent inhibitors of cyclooxygenase-2 as targeted optical imaging agents, *Bioconjug. Chem* 24, 712–723. [PubMed: 23488616]
 33. Uddin MJ, Crews BC, Huda I, Ghebreselasie K, Daniel CK, and Marnett LJ (2014) Trifluoromethyl fluorocoxib A detects cyclooxygenase-2 expression in inflammatory tissues and human tumor xenografts, *ACS Med. Chem. Lett* 5, 446–450. [PubMed: 24900856]
 34. Uddin MJ, Werfel TA, Crews BC, Gupta MK, Kavanaugh TE, Kingsley PJ, Boyd K, Marnett LJ, and Duvall CL (2016) Fluorocoxib A loaded nanoparticles enable targeted visualization of cyclooxygenase-2 in inflammation and cancer, *Biomaterials* 92, 71–80. [PubMed: 27043768]
 35. Uddin MJ, Vemulapalli A, Niitsu H, Crews BC, Oltman CG, Kingsley PJ, Kavanaugh TE, Bedingfield SK, McIntyre JO, Milad M, Aleem AM, Coffey RJ, Duvall CL, and Marnett LJ (2020) Molecular imaging of inflammation in osteoarthritis using a water-soluble fluorocoxib, *ACS Med. Chem. Lett* 11, 1875–1880. [PubMed: 33062167]
 36. Uddin MJ, Moore CE, Crews BC, Daniel CK, Ghebreselasie K, McIntyre JO, Marnett LJ, and Jayagopal A (2016) Fluorocoxib A enables targeted detection of cyclooxygenase-2 in laser-induced choroidal neovascularization, *J. Biomed. Opt* 21, 90503. [PubMed: 27626899]
 37. Cekanova M, Uddin MJ, Legendre AM, Galyon G, Bartges JW, Callens A, Martin-Jimenez T, and Marnett LJ (2012) Single-dose safety and pharmacokinetic evaluation of fluorocoxib A: pilot study of novel cyclooxygenase-2-targeted optical imaging agent in a canine model, *J. Biomed. Opt* 17, 116002. [PubMed: 23117797]
 38. Cekanova M, Uddin MJ, Bartges JW, Callens A, Legendre AM, Rathore K, Wright L, Carter A, and Marnett LJ (2013) Molecular imaging of cyclooxygenase-2 in canine transitional cell carcinomas in vitro and in vivo, *Cancer Prev. Res* 6, 466–476.
 39. Ra H, Gonzalez-Gonzalez E, Uddin MJ, King BL, Lee A, Ali-Khan I, Marnett LJ, Tang JY, and Contag CH (2015) Detection of non-melanoma skin cancer by in vivo fluorescence imaging with fluorocoxib A, *Neoplasia* 17, 201–207. [PubMed: 25748239]
 40. Tondera C, Hauser S, Kruger-Genge A, Jung F, Neffe AT, Lendlein A, Klopffleisch R, Steinbach J, Neuber C, and Pietzsch J (2016) Gelatin-based hydrogel degradation and tissue interaction in vivo: insights from multimodal preclinical imaging in immunocompetent nude mice, *Theranostics* 6, 2114–2128. [PubMed: 27698944]
 41. Shanmugam VK, Tassi E, Schmidt MO, McNish S, Baker S, Attinger C, Wang H, Shara N, and Wellstein A (2015) Utility of a human-mouse xenograft model and in vivo near-infrared fluorescent imaging for studying wound healing, *Int. Wound J* 12, 699–705. [PubMed: 24373153]
 42. Roughan JV, Bertrand HG, and Isles HM (2016) Meloxicam prevents COX-2-mediated post-surgical inflammation but not pain following laparotomy in mice, *Eur. J. Pain* 20, 231–240. [PubMed: 25908253]
 43. Foersch S, Neufert C, Neurath MF, and Waldner MJ (2013) Endomicroscopic imaging of COX-2 activity in murine sporadic and colitis-associated colorectal cancer, *Diagn. Ther. Endosc* 2013, 250641. [PubMed: 23401648]

44. Hou W, Sampath P, Rojas JJ, and Thorne SH (2016) Oncolytic virus-mediated targeting of PGE2 in the tumor alters the immune status and sensitizes established and resistant tumors to immunotherapy, *Cancer Cell* 30, 108–119. [PubMed: 27374223]
45. Uddin MJ, Crews BC, Ghebreselasie K, Daniel CK, Kingsley PJ, Xu S, and Marnett LJ (2015) Targeted imaging of cancer by fluorocoxib C, a near-infrared cyclooxygenase-2 probe, *J. Biomed. Opt* 20, 50502. [PubMed: 25970082]
46. Zhang H, Fan J, Wang J, Zhang S, Dou B, and Peng X (2013) An off-on COX-2-specific fluorescent probe: targeting the Golgi apparatus of cancer cells, *J. Am. Chem. Soc* 135, 11663–11669. [PubMed: 23862760]
47. Yadav AK, Reinhardt CJ, Arango AS, Huff HC, Dong L, Malkowski MG, Das A, Tajkhorshid E, and Chan J (2020) An activity-based sensing approach for the detection of cyclooxygenase-2 in live cells, *Angew. Chem. Int. Ed. Engl* 59, 3307–3314. [PubMed: 31854058]
48. Lee SH, Williams MV, Dubois RN, and Blair IA (2005) Cyclooxygenase-2-mediated DNA damage, *J. Biol. Chem* 280, 28337–28346. [PubMed: 15964853]
49. Onodera Y, Teramura T, Takehara T, Shigi K, and Fukuda K (2015) Reactive oxygen species induce Cox-2 expression via TAK1 activation in synovial fibroblast cells, *FEBS Open Bio*. 5, 492–501.
50. Charalambous MP, Lightfoot T, Speirs V, Horgan K, and Gooderham NJ (2009) Expression of COX-2, NF-kappaB-p65, NF-kappaB-p50 and IKKalpha in malignant and adjacent normal human colorectal tissue, *Br. J. Cancer* 101, 106–115. [PubMed: 19513071]
51. Dikalov SI, Polienko YF, and Kirilyuk I (2018) Electron paramagnetic resonance measurements of reactive oxygen species by cyclic hydroxylamine spin probes, *Antioxid. Redox Signal* 28, 1433–1443. [PubMed: 29037084]
52. Rhodes CJ (2011) Electron spin resonance. Part one: a diagnostic method in the biomedical sciences, *Sci. Prog* 94, 16–96. [PubMed: 21548528]
53. Rhodes CJ (2011) Electron spin resonance. Part two: a diagnostic method in the environmental sciences, *Sci. Prog* 94, 339–413. [PubMed: 22308901]
54. Khodeir M, Ernould B, Brassinne J, Ghiassinejad S, Jia H, Antoun S, Friebe C, Schubert US, Kochovski Z, Lu Y, Van Ruymbeke E, and Gohy JF (2019) Synthesis and characterisation of redox hydrogels based on stable nitroxide radicals, *Soft Matter* 15, 6418–6426. [PubMed: 31338513]
55. Hodgson JL, Namazian M, Bottle SE, and Coote ML (2007) One-electron oxidation and reduction potentials of nitroxide antioxidants: a theoretical study, *J. Phys. Chem. A* 111, 13595–13605. [PubMed: 18052257]
56. Prescott C, and Bottle SE (2017) Biological relevance of free radicals and nitroxides, *Cell. Biochem. Biophys* 75, 227–240. [PubMed: 27709467]
57. Morrow BJ, Keddie DJ, Gueven N, Lavin MF, and Bottle SE (2010) A novel profluorescent nitroxide as a sensitive probe for the cellular redox environment, *Free Radic Biol Med* 49, 67–76. [PubMed: 20350596]
58. Morris JC, McMurtrie JC, Bottle SE, and Fairfull-Smith KE (2011) Generation of profluorescent isoindoline nitroxides using click chemistry, *J Org Chem* 76, 4964–4972. [PubMed: 21545177]
59. Thomas K, Moody TW, Jensen RT, Tong J, Rayner CL, Barnett NL, Fairfull-Smith KE, Ridnour LA, Wink DA, and Bottle SE (2018) Design, synthesis and biological evaluation of hybrid nitroxide-based non-steroidal anti-inflammatory drugs, *Eur J Med Chem* 147, 34–47. [PubMed: 29421569]
60. Yapici NB, Jockusch S, Moscatelli A, Mandalapu SR, Itagaki Y, Bates DK, Wiseman S, Gibson KM, Turro NJ, and Bi L (2012) New rhodamine nitroxide based fluorescent probes for intracellular hydroxyl radical identification in living cells, *Org. Lett* 14, 50–53. [PubMed: 22176578]
61. Enami S, Sakamoto Y, and Colussi AJ (2014) Fenton chemistry at aqueous interfaces, *Proc Natl Acad Sci U S A* 111, 623–628. [PubMed: 24379389]
62. Kehrer JP (2000) The Haber-Weiss reaction and mechanisms of toxicity, *Toxicology* 149, 43–50. [PubMed: 10963860]

63. Smith WL, and Malkowski MG (2019) Interactions of fatty acids, nonsteroidal anti-inflammatory drugs, and coxibs with the catalytic and allosteric subunits of cyclooxygenases-1 and -2, *J Biol Chem* 294, 1697–1705. [PubMed: 30710016]
64. Zhu H, Jia Z, Trush MA, and Li YR (2016) A highly sensitive chemiluminometric assay for real-time detection of biological hydrogen peroxide formation, *React. Oxyg. Species* 1, 216–227.
65. Bedouhene S, Moulti-Mati F, Hurtado-Nedelec M, Dang PM, and El-Benna J (2017) Luminol-amplified chemiluminescence detects mainly superoxide anion produced by human neutrophils, *Am. J. Blood. Res* 7, 41–48. [PubMed: 28804681]
66. di Meglio P, Ianaro A, and Ghosh S (2005) Amelioration of acute inflammation by systemic administration of a cell-permeable peptide inhibitor of NF-kappaB activation, *Arthritis Rheum.* 52, 951–958. [PubMed: 15751079]
67. Griesser M, Shah R, Van Kessel AT, Zilka O, Haidasz EA, and Pratt DA (2018) The Catalytic Reaction of Nitroxides with Peroxyl Radicals and Its Relevance to Their Cytoprotective Properties, *J Am Chem Soc* 140, 3798–3808. [PubMed: 29451786]
68. Harrison KA, Haidasz EA, Griesser M, and Pratt DA (2018) Inhibition of hydrocarbon autoxidation by nitroxide-catalyzed cross-dismutation of hydroperoxyl and alkylperoxyl radicals, *Chem Sci* 9, 6068–6079. [PubMed: 30079220]

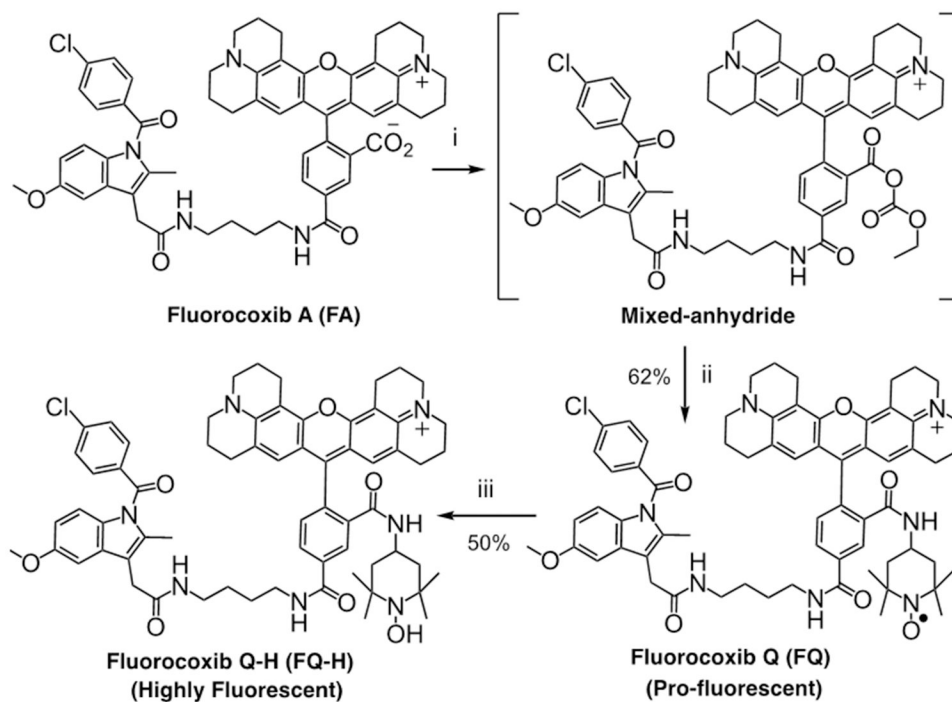


Figure 1. Synthesis of FQ.

(i) Ethyl chloroformate, triethylamine, tetrahydrofuran, $-15\text{ }^{\circ}\text{C}$, 1 h; (ii) 4-amino-2,2,6,6-tetramethyl-1-piperidynitroxide free radical, tetrahydrofuran, $-15\text{ }^{\circ}\text{C} \rightarrow 25\text{ }^{\circ}\text{C}$, 16 h; (iii) ascorbic acid, water, $25\text{ }^{\circ}\text{C}$, 16 h.

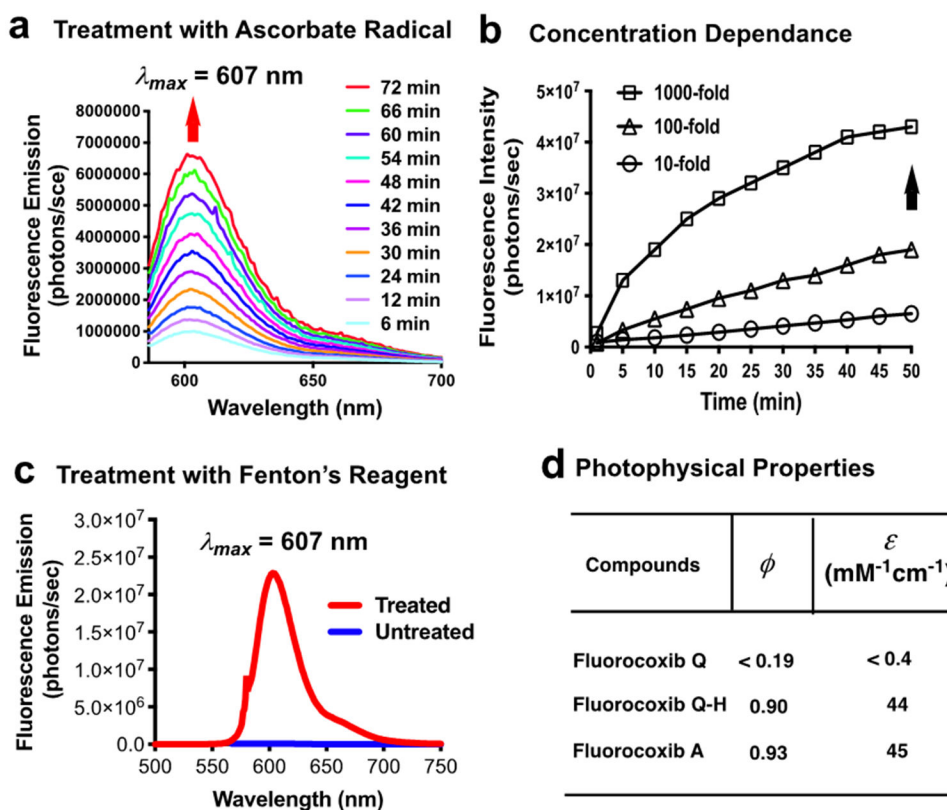


Figure 2. Properties of FQ.

(a) Time dependent fluorescence increase of FQ on sodium ascorbate treatment (1:1) in buffer pH 7.4; (b) effect of increased concentration of sodium ascorbate on fluorescence increase of FQ; (c) fluorescence spectra of FQ before and after treating with Fenton reagent (Fe^{2+} : H_2O_2 , mol/mol = 1:10); (d) quantum yield and molar extinction coefficient of FQ and FQ-H.

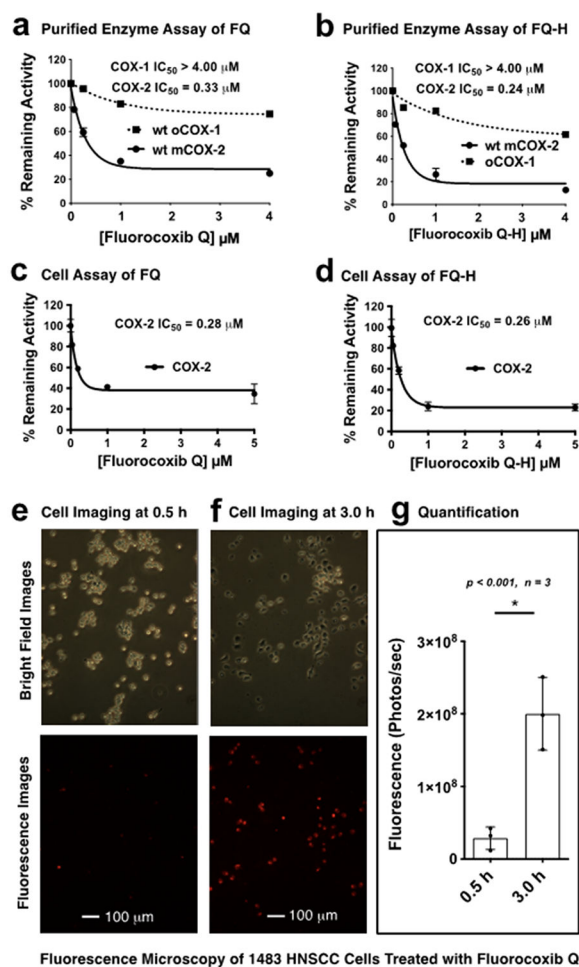
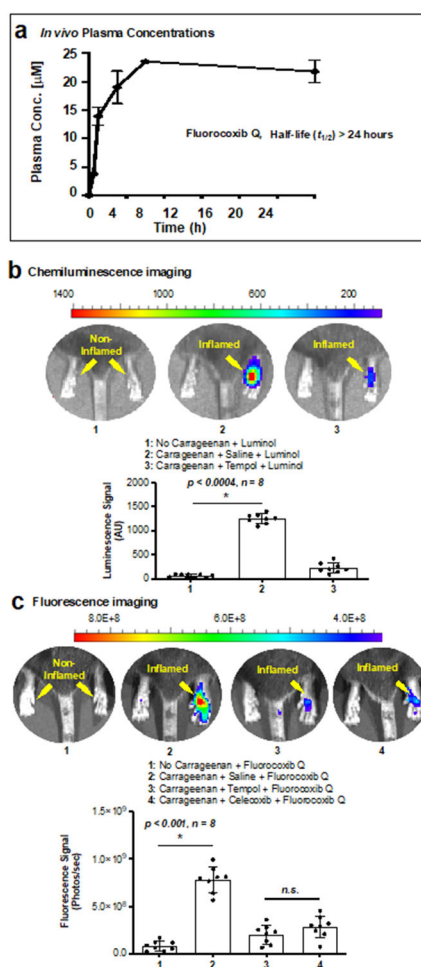


Figure 3. Evaluation of FQ.

(a,b) Purified α COX-1 and mCOX-2 isozyme inhibition by FQ and FQ-H, respectively; (c,d) cell-based (1483 HNSCC cells) COX-2 inhibition by FQ and FQ-H, respectively; (e-f) 1483 HNSCC cells were treated with FQ followed by fluorescence microscopy at 0.5 h and 3 h post-incubation; (g) cell fluorescence was measured on a BioTek Synergy MX Plate Reader, and Welch's correction was performed for an unpaired parametric t test performed to assess statistical difference, where the error bars represent standard error.

**Figure 4.**

In vivo experiments. FQ plasma concentration versus time is shown in (a); the half-life exceeds 24 h. (b-c) chemiluminescence imaging of carrageenan-induced mouse footpad inflammation using luminol with saline or TEMPOL pre-treated animals, and fluorescence imaging of mouse footpad inflammation using FQ with saline, TEMPOL or celecoxib pre-treated animals. We used an ImageJ software to measure fluorescence at the regions of interest. We performed a Welch's correction to assess statistical difference. The error bars represent standard error and n.s. stand for not significant.